Comparisons of Models for Simulating Energy Transfer in Ne-Atom Collisions with an Alkyl Thiolate Self-Assembled Monolayer†

Tianying Yan and William L. Hase*

Institute for Scientific Computing, Department of Chemistry, Wayne State University, Detroit, Michigan 48202

Received: April 5, 2002; In Final Form: June 12, 2002

A range of attributes of a molecular dynamics model for Ne-atoms colliding with a *n*-hexylthiolate self-assembled monolayer (SAM)/Au{111} surface are investigated to determine how they affect the energy-transfer dynamics. Explicit-atom (EA) and united-atom (UA) models for the SAM surface give similar energy accommodation, with energy transfer to the EA model approximately 10% less efficient. An accurate potential energy function is needed to described the interaction between Ne and the carbon and hydrogen atoms of the SAM. Quasiclassical and molecular dynamics sampling of initial conditions for the SAM give very similar simulation results. A SAM model with only 35 alkyl chains gives the same energy transfer to the Au{111} substrate as do much larger models. Energy transfer to the Au{111} substrate is unimportant during the Ne-atom collision. Increasing the temperature of the SAM in the initial conditions and, thus, increasing the SAM's thermal motion lead to more energy dissipation pathways and broaden the energy-transfer distribution function. As found in previous work, the apparent Boltzmann component in this distribution does not arise from a trapping desorption intermediate.

I. Introduction

Self-assembled monolayers (SAMs) are long-chain functionalized molecules self-standing on the surface of solid.[1−4] In the past decade, SAMs have attracted much attention in experiments as well as in computer simulations regarding their phase behavior,[5−7] friction,[8−10] and energy-transfer dynamics when struck by projectiles.[11−14] Recent experiments have been performed of Ne collisions with the octadecyltrichlorosilane (OTS) SAM on an oxidized Si(001) substrate[15] and Ne and Ar collisions with a decanethiolate SAM on a Au{111} substrate.[16]

In gas−surface collisions, trapping is used to denote sticking of an incoming particle to the surface. Statistical theories are widely used to interpret of the dynamics of collision processes that proceed through intermediates.[17] A statistical intermediate in a gas−surface collision has a sufficiently long residence time on the surface to thermally equilibrate with the surface and forget its incident energy and direction. Thus, its desorption dynamics is identical to surface effusion at a certain temperature. The statistical translational energy distribution for a species desorbing from a surface is the Maxwell−Boltzmann distribution

$$P(E_f) = (k_b T_S)^{-2} E_f \exp(-E_f/(k_b T_S)) \quad (1)$$

where E_f is the final translational energy of the scattered particle, T_S is the surface temperature, and k_b is Boltzmann's constant. The average translational energy given by eq 1 is $2k_bT_S$/mol. Equation 1 also applies to molecules effusing through a small hole into a vacuum.[18] The other type of limiting gas−surface collision is direct inelastic scattering, for which the projectile rebounds directly off the surface with just one inner turning point in the gas−surface collision.[19,20]

It is difficult, if not impossible, to observe the trapped/desorbed particles experimentally. Therefore, trapping desorption is often identified in experiments by observing gas−surface scattering in accord with eq 1. The fraction of trapping is then associated with the fraction of the scattered particle's translational energy distribution, $P(E_f)$, that can be fit by eq 1.[21] In trajectory simulations of gas−surface collisions, a variety of criteria have been used to identify trapping. One is the presence of multiple inner turning points (MITPs) in the projectile's motion perpendicular to the surface.[22−24] The energy of the colliding species has also been used as a criterion of trapping. Here, the colliding species is assumed to be trapped if its energy falls below some critical value, for example, its adsorption well-depth.[25−28]

In our previous studies of Ne + SAM collisions,[12−14] classical trajectory simulations were used to study the dynamics of Ne-atom scattering off a *n*-hexylthiolate SAM absorbed on a Au{111} surface. It is possible to deconvolute the trajectory $P(E_f)$ into one component accurately represented by Boltzmann distribution in eq 1 based on the temperature higher than the surface temperature[26] and a remaining non-Boltzmann high-energy component. However, in contrast to the long residence time required for thermalization, the residence time of a Ne + *n*-hexylthiolate SAM hyperthermal collision is quite short, about 0.5−1 ps, and most trajectories are directly scattered off the SAM with no MITPs.[13,29] It is notable that the adsorption well-depth of Ne with the SAM is quite small, which is different than other gas−surface scattering systems in which the binding energy is large. Therefore, for the most part, the Ne-atoms scatter off the SAM without trappings. This is consistent with the experiments of Cl(^{2}P) and O(^{3}P) scattering off a hydrocarbon surface performed by Minton et al.,[30,31] in which direct scattering is dominant and can be viewed as the atom interacting with an effective surface mass and a kinematic picture given by the Newton diagram.[32] Given these dynamics, it is somewhat

† Part of the special issue "John C. Tully Festschrift".

* To whom correspondence should be addressed. E-mail: wlh@chem.wayne.edu.

10.1021/jp025902w CCC: $22.00
Published on Web 07/09/2002

surprising to find a large Boltzmann channel in the final Ne translational energy distribution.

For the study presented here, different models are used to represent the Ne + SAM/Au{111} system to establish the sensitivity of the previous trajectory results to the simulation model. The following attributes of the models are considered: (1) a comparison of united-atom (UA) and explicit-atom (EA) representations of the SAM; (2) effect of increasing the number of *n*-hexylthiolate chains used to represent the SAM surface; (3) effect of adjusting the Ne−SAM adsorption well depth and short-range repulsion and modifying the potential energy function for the Ne + SAM interaction; (4) a comparison of selecting 300 K initial conditions for the SAM by quasiclassical[33,34] and molecular dynamics sampling;[35] (5) a consideration of different approaches for treating the Au{111} surface as a thermal bath.

II. Computational Details

A. Surface Model. *1. UA and EA Models for the SAM.* Two types of models were investigated for the SAM. One is the united-atom (UA) model used in our previous work[12,13] in which a pseudo-atom is used for the methyl and methylene groups of the hexyl chains. Well-established analytic functions and parameters[36] are used for the inter- and intramolecular potentials of the chains. An explicit-atom (EA) model for the SAM, in which the hydrogen atoms are included, is also considered here. Details of the EA model were presented previously.[37,38] Both surface models consist of $CH_3(CH_2)_5S$ chains adsorbed on a Au{111} surface by bonding the sulfur atoms to 3-fold hollow sites on the surface as described previously.[12] The resulting SAM monolayer forms a commensurate $\sqrt{3} \times \sqrt{3}R30°$ structure, which has after energy minimization a 22°−30° "tilt angle" between the Au{111} surface normal and the backbone of the $CH_3(CH_2)_5S$ moiety, which is in good agreement with the experimental measurements.[39,40]

One UA model for the SAM, identified here as a small model, is the model used previously. It consists of 35 *n*-hexylthiolate chains chemisorbed on a Au{111} surface composed of 127 Au atoms (see Figure 1 in ref 12). To study how the size of the SAM model affects the energy-transfer dynamics, a large UA model of 100 chains chemisorbed on a 325-atom gold surface was also investigated; see Figure 1b. To ensure flatness of the Au surface, a gold anchor atom directly below the surface is used. Interactions between neighboring Au atoms on the surface and between the anchor and surface atoms are modeled by a harmonic stretch potential with a fictitious large force constant of 125 mdyn/Å to maintain a planar surface. These two UA models are identified as UA-small/Au-1-stiff and UA-large/Au-1-stiff, where Au-1-stiff denotes a single-layer and stiff-potential model for the gold surface. An EA model, called EA-small/Au-1-stiff, is considered. It is identical to the UA-small model, except the above explicit-atom model is used for 35 chains (see Figure 1a).

Two modifications were made to the UA-small/Au-1-stiff model to study their effects on the simulations. For one, the gold layer is coupled to a 293 K Berendsen heat bath.[41] This model is called UA-small/Au-1-stiff(bath). For the second model, identified by UA-small/Au-1-rigid, the Au atoms are rigid and kept in their minimum energy structure by not including their coordinates and momenta in the simulation. The S atoms interact with but do not exchange energy with the Au atoms.

2. Two-Layer Gold Model. To determine whether a larger model for the Au{111} surface would affect the energy-transfer dynamics, a two-layer model was used in conjunction with the UA-small model for the SAM surface. The inner Au layer, attached to the $CH_3(CH_2)_5S$ chains, was either treated the same as the SAM surface or as a Berendsen bath, while the outer layer was kept rigid as described above. The inner and outer layers consist of 126 and 103 atoms, respectively. The structure of the model is identical to that of the single-layer model (see Figure 1 in ref 12), except that there is a second Au-atom layer.

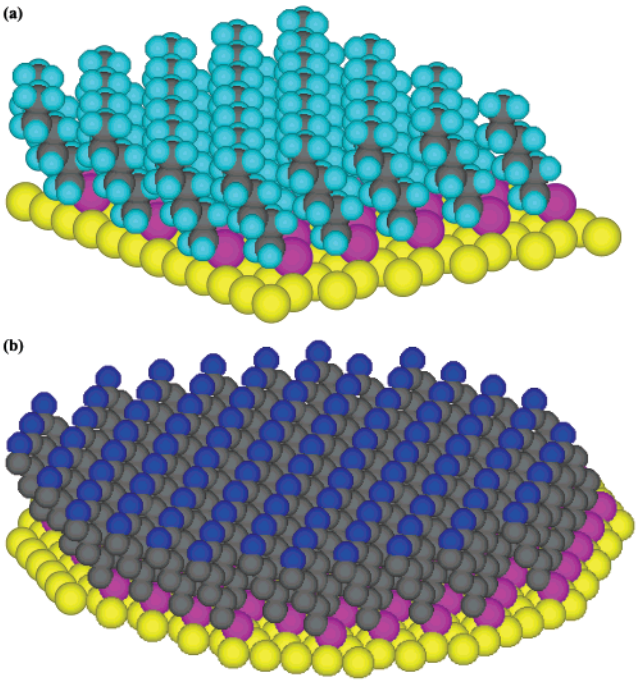

Figure 1. Surface model with (a) 35 $CH_3(CH_2)_5S$ chains and one gold layer with 127 atoms and (b) 100 $CH_3(CH_2)_5S$ chains and one gold layer with 325 atoms.

Two different models are used to represent the potential between the Au atoms in the inner layer and between those in the inner and outer layers. One is the universal force field (UFF),[42] in which a harmonic potential with a force constant of 1.98 mdyn/Å is used between neighboring atoms. The system model with this potential is called UA-small/Au-2-UFF.

It is well-known that in crystalline and metallic materials the electron density plays a dominant role in interactions between atoms and often a quantitative representation of physical properties is not possible with simple pairwise interactions. To determine whether a more-detailed Au{111} potential would affect the simulation results, the two-layer gold model was also represented by the many-body semiempirical Sutton−Chen interatomic potential:[43,44]

$$V_{tot} = \sum_i V_i = \sum_i \epsilon[(^1/_2)\sum_{j\neq i} V(r_{ij}) - c\sqrt{\rho_i}] \qquad (2)$$

where

$$V(r_{ij}) = (a/r_{ij})^n \qquad (3)$$

$$\rho_i = \sum_{j\neq i} (a/r_{ij})^m \qquad (4)$$

Here, n and m are positive integers, c is a dimensionless term, and ϵ is a parameter with the dimension of energy. The above four parameters are fit to bulk elastic quantities with a, the fcc lattice constant. The first term in eq 2 describes the core repulsion, and the second term describes the bonding mediated

by the electrons. The parameters for Au are $\epsilon = 0.295$ kcal mol^{-1}, $c = 34.408$, $m = 8$, $n = 10$, and $a = 4.08$ Å. The Sutton−Chen potential may be rewritten to resemble a simple pair potential[45]

$$V = \sum_{i=1}^{N-1}\sum_{j>i}^{N}\epsilon[a^n r_{ij}^{-n} - ca^m(\rho_i^{-1/2} + \rho_i^{-1/2})r_{ij}^{-m}] \qquad (5)$$

This shows that the surface atom that is in a low-density environment is more strongly attracted to its neighbors than an atom in the bulk, because ρ_i for an atom on the surface is smaller than that for an atom in the bulk. The system model with the Sutton−Chen potential is called UA-small/Au-2-SC.

B. Ne−SAM Potential. In the previous simulations, the intermolecular potential between the colliding Ne atom and the carbon and hydrogen atoms of the $CH_3(CH_2)_5S$ chains was modeled by the Ne + CH_4 potential, calculated at the QCISD-(T)/6-311++G** level of theory. In the work presented here, the Ne + CH_4 potential remains a basis for the Ne + SAM potential, but additional ab initio calculations[46] and fitting functions are used to represent the Ne + CH_4 potential.

1. Ab Initio Ne + CH_4 Potentials. Ab initio potential energy curves were calculated for Ne interacting with (1) the CH_3 *face* of CH_4 and along the Ne···H_3CH C_{3v} axis, (2) an *edge* of CH_4 and bisecting a H−C−H angle along a C_{2v} axis, and (3) a *vertex* configuration along the Ne···HCH_3 C_{3v} axis. In our previous work, the potential for the face configuration was determined at the QCISD(T)/6-311++G** level with full counterpoise (CP) correction to account for basis set superposition error (BSSE).[47] Here, these calculations are extended to include the edge and vertex configurations. The potential energy curves and potential energy minima well depth and Ne−C separations for these configurations are given in Figure 2 and Table 1, respectively.

The MP4 level of theory, which is capable of recovering over 95% of the electron correlation contribution to the intermolecular energy and which gives a result comparable to CCSD(T),[48] was also used to determine the Ne + CH_4 potential curves. The calculations were performed with the aug-cc-pVTZ basis set and full CP correction to account for BSSE. The results of these calculations are given in Figure 2 and Table 1. Also listed in Table 1 are the results of previous MP3[49] and MP4[50] calculations for the Ne−CH_4 potential energy minima. These MP4 calculations were performed with a large basis set, similar to the one used for the MP4 calculations reported here, and the two sets of MP4 results are nearly identical. The results of the MP3 calculations with a BSSE correction included are similar to those determined at the MP4 level of theory, but neglecting this correction results in potential energy well depth that is too deep.

The MP4 calculations give well depths and Ne−C separations for the potential energy minima in excellent agreement with those of a potential energy function derived from the experimental results of Buck et al.[51] The well depth of the face configuration for the previous QCISD(T)[12] calculation is approximately −0.1 kcal/mol and too shallow compared to the MP4 calculations and the experimental result.

2. EA Analytic Functions for Ne−C and Ne−H Potentials. Several different schemes were used to fit the above ab initio Ne−CH_4 potential energy curves to develop EA and UA models for neon interacting with carbon and hydrogen atoms of the $CH_3(CH_2)_5S$ chains. EA potentials were determined by simultaneously fitting either QCISD(T) or MP4 curves in Figure 2 with the equation

$$V(r_{ij}) = A\exp(-Br_{ij}) + C/r_{ij}^{n} \qquad (6)$$

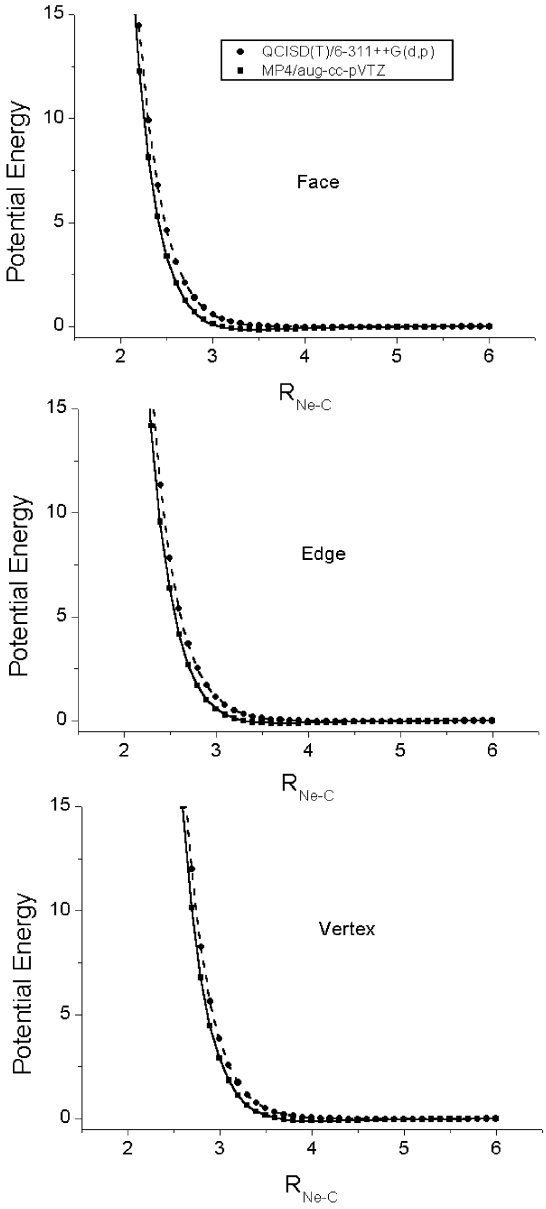

Figure 2. Comparison of QCISD(T)/6-311++G(d,p) and MP4/aug-cc-pVTZ potential curves for Ne + CH_4. The fits for those two sets of curves are given by Ne-IV and Ne-V, respectively. Potential energy is in kcal/mol and distance in Å.

Four different EA potentials, identified as Ne-I, Ne-II, Ne-III, and Ne-IV, were developed from the MP4 potential energy curves. Ne-I is derived by only fitting the face and vertex potentials, and an excellent fit is obtained. For Ne-II, the edge potential is included in the fit, which, as shown in Figure 3, is only approximate.

A more accurate fit is obtained by including Ne−C−H three-body interactions, represented by the Axilrod−Teller (AT)[52] potential

$$V_{ijk} = Z\frac{1 + a\cos\alpha_i\cos\alpha_j\cos\alpha_k}{(r_{ij}r_{ik}r_{jk})^3} \qquad (7)$$

where the α's are the three angles of the triangle defined by the positions of Ne, C, and H atoms atoms and r_{ij}'s are the sides of the triangle. Z and a are the nonadditive coefficients. Two approaches were used to include eq 7 in the fit. For the Ne-III potential, only the three Ne−C−H triangles for the face

TABLE 1: Ab Initio Calculations of the Ne + CH_4 Potential Minima

level of theory	basis set	BSSE correction	face		edge		vertex		ref
			V_{min}[a]	R_{Ne-C}[b]	V_{min}	R_{Ne-C}	V_{min}	R_{Ne-C}	
QCISD(T)	6-311++G(d,p)	Y	−0.02	4.1	−0.01	4.4	−0.01	4.7	this work
MP3	6-31G(3d,3p)	Y	−0.09	3.6	−0.06	3.9	−0.06	4.2	49
MP3	6-311++G(3d,3p)	N	−0.44	3.3	−0.32	3.5	−0.39	3.9	49
MP4	*c*	Y	−0.17	3.5	−0.12	3.5	−0.10	4.0	50
MP4	aug-cc-pVTZ	Y	−0.15	3.5	−0.12	3.7	−0.09	4.1	this work
exptl results[d]			−0.15	3.4	−0.15	3.6	−0.09	4.1	50

[a] Unit in kcal/mol. [b] Unit in Å. [c] [6s4p] contracted from [14s9p] for C, [8s5p] contracted from [14s10p] for Ne, [5s] contracted from [10s] for H, and extended with different polarization functions.[50] [d] By U. Buck et al., referred as private communications in 1997.[50]

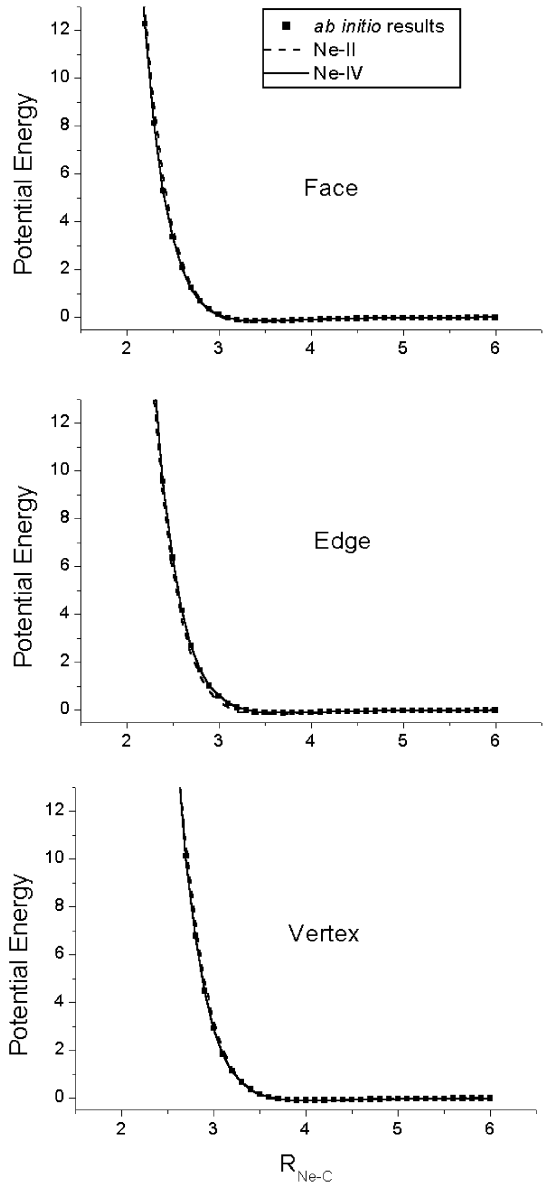

Figure 3. Comparison of fits to the MP4/aug-cc-pVTZ potential curves by the Ne-II and Ne-IV model. Ne-III gives a fit intermediate to those of Ne-II and Ne-IV. Potential energy is in kcal/mol and distance in Å.

configuration are included in eq 7. This model is developed to represent Ne interacting with the CH_3 moiety of the alkyl chain. For Ne-IV, developed to derive a UA model (see below), all four Ne−C−H angles are included in eq 7. The parameters for the four potentials are listed in Table 2. The fits to the face, vertex, and edge Ne−CH_4 potential curves by the Ne-II and Ne-IV function are shown in Figure 3. The fits to the face and vertex potentials by Ne-I are not shown, and they are nearly identical to those in Figure 3 for the Ne-IV function.

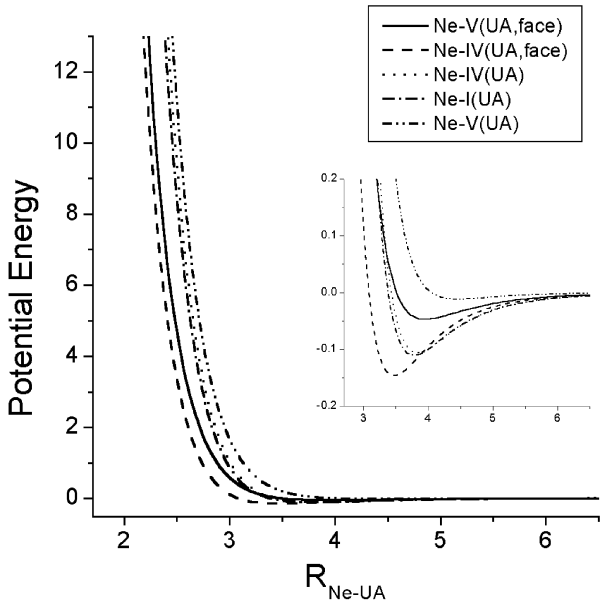

Figure 4. Comparison of Ne-UA potential energy curves. Potential energy is in kcal/mol and distance in Å.

The Ne-V potential is the same type of function as Ne-IV except that the fit is to the QCISD(T) calculations. The parameters for Ne-V are given in Table 2, and its fit is shown in Figure 2.

3. Ne-UA Potential Functions. The analytic function used to describe the interaction between Ne and either a CH_3 or CH_2 united atom (UA) is the same as that used previously[12] and a sum of Lennard-Jones and Buckingham terms, that is,

$$V(r) = A/r^{12} + B/r^6 + C\exp(-Dr) + F/r^9 \qquad (8)$$

In all of our previous simulations,[12−14] the Ne-UA potential was represented by the QCISD(T)/6-311++G** potential energy curve for the Ne−H_3CH face configuration. This potential is identified as Ne-V(UA,face). Additional UA models were developed by assuming that the Ne−CH_3 (UA) and Ne−CH_2 (UA) interactions are the same as the isotropic Ne−CH_4 interaction. Three Ne-UA potentials of this type were determined from the Ne-I, Ne-IV, and Ne-V EA potentials described above and are named Ne-I(UA), Ne-IV(UA), and Ne-V(UA). To calculate the isotropic Ne−CH_4 interaction from these EA potentials, CH_4 is held rigid in its equilibrium geometry and then randomly rotated to calculate the average Ne−CH_4 potential as a function of the Ne−C distance. A UA model only based on the MP4 face potential is also considered, and it is called Ne-IV(UA,face). Each of the five Ne-UA potentials are plotted in Figure 4 and their parameters are listed in Table 3.

The well depth (kcal/mol) and Ne-UA separation (Å) at the potential energy minima for the Ne-I(UA), Ne-IV(UA), Ne-V(UA), Ne-IV(UA,face), and Ne-V(UA,face) potentials are

TABLE 2: Explicit-Atom Analytic Fits to the ab Initio Calculations

	generalized exponential two-body terms								Axilrod−Teller three-body terms	
	Ne−C				Ne−H				Ne−C−H	
function[a]	A[b]	B[c]	C[d]	n	A	B	C	n	Z[e]	a
Ne-I	93 336.7	4.03	−4364.8	8.77	6371.7	3.79	−84.5	5.97	*f*	*f*
Ne-II	150 621.6	3.96	−28243.6	9.50	12 005.3	3.90	−370.7	7.10	*f*	*f*
Ne-III	177 027.9	4.04	−27153.3	9.36	9806.4	3.79	−306.7	6.92	31.43	3
Ne-IV	107 570.8	3.98	−5128.9	6.26	3291.7	3.53	−43.3	6.04	1104.7	0.45
Ne-V	70 203.9	3.88	−4235.4	6.02	4877.3	3.78	−117.6	6.22	1430.7	0.18

[a] Ne-I−IV are fits to the MP4/aug-cc-pVTZ calculations and, Ne-V is fit to QCISDT/6-311++G(d,p) ab initio calculations. [b] Unit in kcal mol^{-1}. [c] Unit in Å^{-1}. [d] Unit in Å^{-n} mol^{-1}. [e] Unit in kcal Å^{9} mol^{-1}. [f] Term is not used.

TABLE 3: Ne−CH_4(UA) Potential Models

		Lennard-Jones + Buckingham terms				
function	level of theory	A[a]	B[b]	C[c]	D	F[d]
Ne-IV(UA,face)	MP4/aug-cc-pVTZ	23 679.3	−317.3	95 135.0	3.79	−11 399.5
Ne-V(UA,face)[e]	QCISD(T)/6-311++G(d,p)	−2 660.5	−320.4	40 710.0	3.53	496.6
Ne-I(UA)	MP4/aug-cc-pVTZ	−65 899.8	−393.1	182 231.1	3.77	−13 468.3
Ne-IV(UA)	MP4/aug-cc-pVTZ	62 260.3	−365.2	136 282.3	3.64	−20 907.6
Ne-V(UA)	QCISD(T)/6-311++G(d,p)	−7 280.5	−69.7	131 197.4	3.66	−9 514.1

[a] Unit in Å^{12} kcal mol^{-1}. [b] Unit in Å^{6} kcal mol^{-1}. [c] Unit in kcal mol^{-1}. [d] Unit in Å^{9} kcal mol^{-1}. [e] Parameters are taken from ref 12.

(−0.11, 3.80), (−0.11, 3.84), (−0.01, 4.55), (−0.15, 3.50), and (−0.05, 3.95), respectively. The properties of the potential energy minima for the former two potentials are in excellent agreement with experiment. The crossed molecular beam study of Buck et al. gives a Ne−CH_4 complex with an average Ne−C separation of 3.83 ± 0.06 Å and potential energy of −0.11 kcal/mol.[51] A similar experiment by Liuti et al. gives 3.78 Å and −0.13 kcal/mol for these two properties.[53] A recent vibrational−rotational spectroscopic study by Wangler et al. gives a B rotational constant of 0.129 cm^{-1} for the Ne−CH_4 complex, corresponding to an average Ne−C separation of 3.8 Å and a nearly freely rotating CH_4 molecule.[54]

C. Classical Trajectory Simulations. The classical trajectory simulations are carried out with the general chemical dynamics computer program VENUS.[55] The algorithm for choosing initial conditions for the trajectories is standard options in VENUS, and initial coordinates for a beam of Ne atoms are chosen according to the sampling method described previously.[12] The initial translational energy, E_i, and polar angle, θ_i, of the beam are fixed at 10 kcal/mol and 45°. The azimuthal angle, χ_i, the projection of the incident beam onto the SAM surface, is chosen randomly between 0° and 360° to represent collision with different domains of growth on the surface.[12] These conditions are representative of those in previous simulations and experiment.

It is of interest to determine whether the Ne + SAM/Au{111} trajectory is sensitive to the method for choosing initial conditions for the SAM, and for the simulations with the small united-atom SAM model UA-small/Au-1-stiff, both quasiclassical normal mode sampling[33,34] and molecular dynamics (MD) sampling[35] are used to choose initial conditions for the SAM. For the large surface models, only MD sampling is used for the SAM.

Both the quasiclassical and MD sampling methods have been described previously.[12,38] In quasiclassical sampling, the normal modes of vibration for the surface are calculated and the quantum energy levels are sampled for each normal mode in accord with its 293 K Boltzmann distribution. For the 373 atoms of the UA-small/Au-1-stiff model, this includes more than 1000 kcal/mol of zero-point energy. A random phase is then chosen for each normal mode, and the normal mode eigenvector is used to transform the normal mode coordinates and momenta to the Cartesian coordinates and momenta used for the trajectory simulation. In MD sampling, standard classical molecular dynamics is used to prepare the surface in an equilibrium state with a temperature of approximately 293 K. The surface then forms a classical canonical ensemble as it evolves in time and initial Cartesian coordinates and momenta for the surface are selected at a random time in this evolution.

TABLE 4: Effect of Different EA Models for the Ne−SAM Potential[a]

Ne−SAM potential	$\langle E_f \rangle$[b]	%BC[c]	T_{BC}[d]	%MITPs[e]	$\langle E_f \rangle_{MITPs}$[f]
Ne-I	3.33 ± 0.18[g]	70.0	615	5.6	1.83 ± 0.39
Ne-II	3.25 ± 0.19	72.0	605	7.1	1.90 ± 0.45
Ne-II+III	3.25 ± 0.16	56.5	475	9.6	1.79 ± 0.30

[a] The surface model is EA-small/Au-1-stiff, and initial conditions for the SAM are chosen by MD sampling. [b] Average final energy of scattered Ne-atoms in kcal/mol. [c] BC is the Boltzmann component and %BC is the percent of $P(E_f)$ that is represented by eq 1. [d] Temperature (K) for Boltzmann component, eq 1, of $P(E_f)$. [e] Percent of the trajectories with multiple inner turning points (MITPs). [f] $\langle E_f \rangle$ for trajectories with MITPs. [g] Uncertainty is for a 95% confidence interval.

The differences between these two sampling methods are well-known and have been discussed previously.[56] Quasiclassical sampling approximates a quantum canonical ensemble by sampling Boltzmann distributions for the normal modes defined by the potential energy minimum of the SAM. The sampling does not account for anharmonicity or multiple potential minima, which arise in part from the dihedral angles of the $CH_3(CH_2)_5S$ chains of the SAM. In MD sampling, a true 293 K classical canonical ensemble is formed, which randomly samples all of the potential minima. If the system was harmonic, the average energy in each mode would be *RT*. In contrast, for quasiclassical sampling, the average mode energy is higher than *RT* because zero-point energy is added. If all of the energy added to the SAM in quasiclassical sampling becomes randomized, the classical temperature of the SAM would be approximately 600 K.

The information collected from each trajectory is the final translational energy, E_f, of the scattered Ne atom and the number of multiple inner turning points (MITPs) of the motion of the Ne atom with respect to the SAM. The trajectories are not sorted by the scattering angles of the Ne atoms.

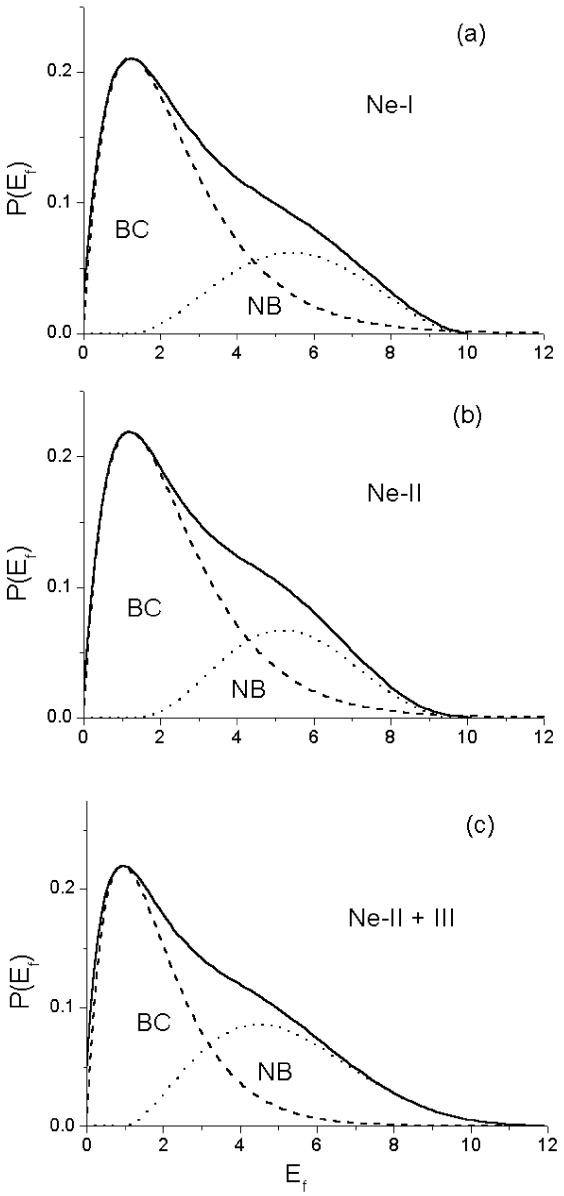

Figure 5. Energy-transfer distribution for Ne scattering with different EA models for the Ne + SAM interaction. The surface for the simulation is EA-small/Au-1-stiff, and 293 K MD sampling is used to choose initial conditions for the surface. BC and NB are Boltzmann and non-Boltzmann components to $P(E_f)$. Energy is in kcal/mol.

III. Results and Discussion

A. Effect of the Ne−SAM Model and Potential Energy Function. *1. EA Models for the SAM.* Energy transfer was compared using the Ne-I, -II, and -III EA functions, described in section II.B.2, for the Ne−SAM potential. Each is a different fit to the MP4/aug-cc-pVTZ calculations for the Ne−CH_4 interactions. Ne-I is a two-body fit to the face and vertex potential energy curves, Ne-II a two-body fit to the face, vertex, and edge potential curves, and Ne-III a two-body + three-body fit to all three of these curves with only the three Ne−C−H angles associated with the Ne−H_3CH face configuration included in the three-body Axilrod−Teller function. Three different simulations were performed using these potentials. For the first, the Ne−H and Ne−C potentials for the Ne−SAM interaction are represented by Ne-I, and for the second simulation, they are represented by Ne-II. For the third simulation, the potentials for Ne interacting with CH_3 are represented by Ne-III and by Ne-II for Ne interacting with CH_2. Each

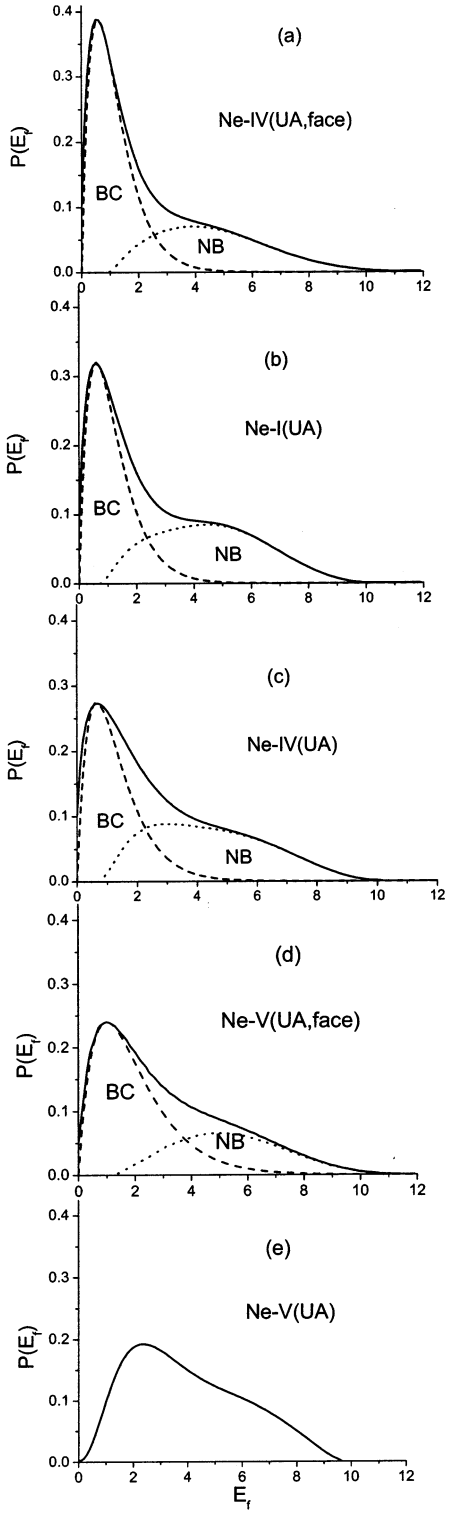

Figure 6. Energy-transfer distribution for Ne scattering with different UA models for the Ne + SAM interaction. The surface is UA-small/Au-1-stiff, and quasiclassical sampling is used to choose initial conditions for the surface. BC and NB are Boltzmann and non-Boltzmann components to $P(E_f)$. Energy is in kcal/mol.

simulation was performed with the EA-small/Au-1-stiff model for the surface and MD sampling to select initial conditions for the SAM.

As shown in Table 4 and Figure 5, these three simulations give very similar Ne + SAM energy-transfer dynamics. The only significant difference is that the Ne-II+III model has a somewhat smaller Boltzmann component and associated tem-

TABLE 5: Effect of Different UA Models for the Ne−SAM Potential[a]

SAM potential[b]	Ne−UA well depth[c]	$\langle E_f \rangle$[d]	%BC[d]	T_{BC}[d]	%MITPs[d]	$\langle E_f \rangle_{MITPs}$[d]
Ne-IV(UA,face)	−0.15	2.44 ± 0.14[e]	61.5	290	23.4	1.22 ± 0.13[e]
Ne-I(UA)	−0.11	2.78 ± 0.14	53.0	300	7.2	0.79 ± 0.15
Ne-IV(UA)	−0.11	2.86 ± 0.10	50.0	330	5.1	0.73 ± 0.12
Ne-V(UA,face)	−0.05	3.16 ± 0.13	65.0	500	1.0	*f*
Ne-V(UA)	−0.01	4.10 ± 0.13	0	*f*	0	*f*

[a] Incident energy $E_i = 10$ kcal/mol, incident polar angle $\theta_i = 45°$, and surface temperature $T_s = 293$ K are chosen by quasiclassical sampling. [b] Ne-IV(UA,face), Ne-I(UA), and Ne-IV(UA) are fit to the MP4/aug-cc-pVTZ level of theory. Ne-V(UA,face) and Ne-V(UA) are fit to the QCISD/6-311++G(d,p) level of theory. Details are given in section II.B.3. [c] Unit in kcal/mol. [d] BC is the Boltzmann component and %BC is the percent of $P(E_f)$ that is represented by eq 1. T_{BC} is the temperature (K) for Boltzmann component, eq 1, of $P(E_f)$. %MITPs is the percent of the trajectories with multiple inner turning points (MITPs). $\langle E_f \rangle_{MITPs}$ is the $\langle E_f \rangle$ for trajectories with MITPs. [e] Uncertainty is for a 95% confidence interval. [f] Insignificant number of trajectories or no trajectories.

perature. Using the Ne-III potential for the Ne−CH_3 interaction, instead of Ne-II, gives rise to this rather small effect.

2. UA Models for the SAM. Simulations were performed using the five different UA models described in section II.B.3 for the Ne−CH_3 (UA) and Ne−CH_2 (UA) potentials. The calculations were performed with the UA-small/Au-1-stiff model for the surface and quasiclassical sampling to choose initial conditions for the SAM. The results are given in Table 5 and Figure 6.

The energy-transfer dynamics for the Ne-I(UA) and Ne-IV(UA) potentials are nearly identical. These UA models were determined by isotropic averaging of the potentials for two different EA models of the Ne + CH_4 interaction, each derived from the MP4/aug-cc-pVTZ calculations. As shown above, a similar insensitivity of the results to the particular model used to represent the MP4 calculations is also found for the EA models. The energy-transfer dynamics for the Ne-V(UA,face) potential are similar to those for the Ne-I(UA) and Ne-IV(UA) models. The former has a somewhat larger Boltzmann component with a large $\langle E_f \rangle$ and less trapping, but the difference with the latter two UA potentials is overall rather small. Ne-V(UA,face) is the potential used in all of our previous simulations of the Ne + SAM/Au{111} dynamics. It is a fit to the QCISD(T)/6-311++G(d,p) potential for the Ne−H_3CH face configuration.

The remaining two potentials give significantly different results. Ne-IV(UA,face), which is a fit to the MP4/aug-cc-pVTZ potential for the Ne−H_3CH face configuration and has a rather deep potential energy minimum, gives a smaller $\langle E_f \rangle$ and a much larger percent of MITPs. For Ne-V(UA), which is an isotropic average of the EA model fit to the QCISD(T) potential curves for Ne−CH_4, there is much less energy transfer to the surface and not a well-defined Boltzmann component to $P(E_f)$. This potential has a very shallow Ne-UA potential energy minimum.

3. Large and Small SAM Models. To determine whether increasing the size of the SAM model affects energy transfer to the surface, simulations were compared for the UA-small/Au-1-stiff model with 35 $CH_3(CH_2)_5S$ chains and the UA-large/Au-1-stiff model with 100 $CH_3(CH_2)_5S$ chains. The Ne-IV(UA) potential model was used. MD sampling was used to select initial conditions for the SAM. The results are given in Table 6 and Figure 7. The results are nearly insensitive to increasing the size of the SAM model, which indicates that the 35 chain model is adequate for studying energy transfer in the Ne + SAM/Au{111} collisions.

B. Comparisons of Quasiclassical and MD Sampling for the Surface. The above EA and UA simulations are performed using quasiclassical and MD sampling for the SAM/Au{111} surface, respectively, and it is important to determine the sensitivity of the trajectory results to this sampling. This was done by using the UA-small/Au-1-stiff surface model and the Ne + SAM potential Ne-IV(UA). Calculations were performed for both 293 and 0 K. For the calculations at 0 K, the surface is in its classical potential energy minimum for the MD sampling and in its normal-mode zero-point energy level for quasiclassical

TABLE 6: Effect of Sampling Procedure and Surface Size for Simulations with the Ne-IV(UA) Potential Model

sampling	surface	$\langle E_f \rangle$[b]	%BC[b]	T_{BC}[b]	%MITPs[b]	$\langle E_f \rangle_{MITPs}$[b]
QC, 293[a]	UA-small	2.86 ± 0.11[c]	50.0	330	5.1	0.73 ± 0.12[c]
MD, 293[a]	UA-small	2.65 ± 0.13	67.5	420	9.4	1.54 ± 0.26
MD, 293[a]	UA-large	2.57 ± 0.12	69.0	420	12.9	1.30 ± 0.17
QC, 0[a]	UA-small	2.80 ± 0.11	54.5	330	1.4	*d*
MD, 0[a]	UA-small	2.55 ± 0.11	0	*d*	1.0	*d*

[a] Initial temperature (K) of the surface. [b] BC is the Boltzmann component and %BC is the percent of $P(E_f)$ that is represented by eq 1. T_{BC} is the temperature (K) for Boltzmann component, eq 1, of $P(E_f)$. %MITPs is the percent of the trajectories with multiple inner turning points (MITPs). $\langle E_f \rangle_{MITPs}$ is the $\langle E_f \rangle$ for trajectories with MITPs. [c] Uncertainty is for a 95% confidence interval. [d] Insignificant number of trajectories.

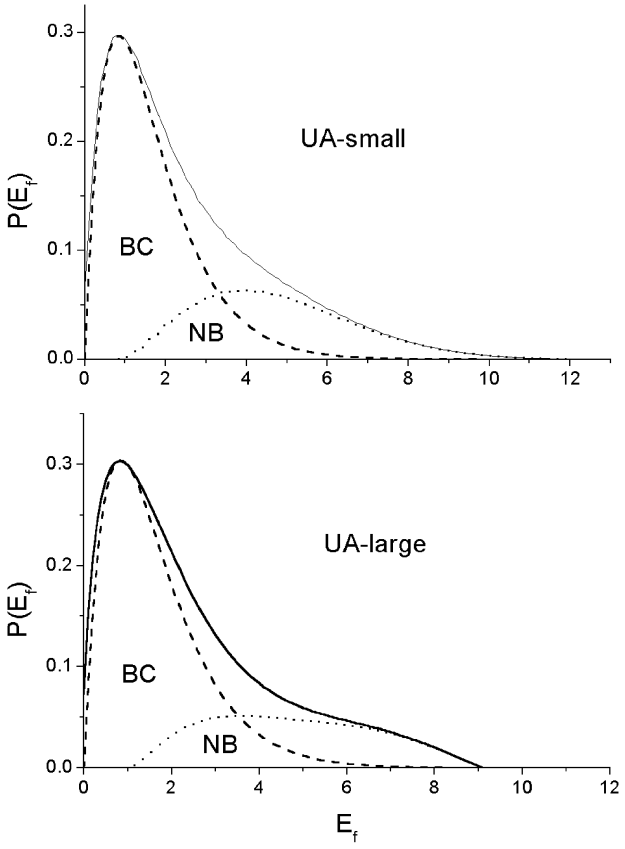

Figure 7. Comparison of small and large UA model for the SAM, using the Ne-IV(UA) potential, the Au-1-stiff model, and 293 K MD sampling for the surface.

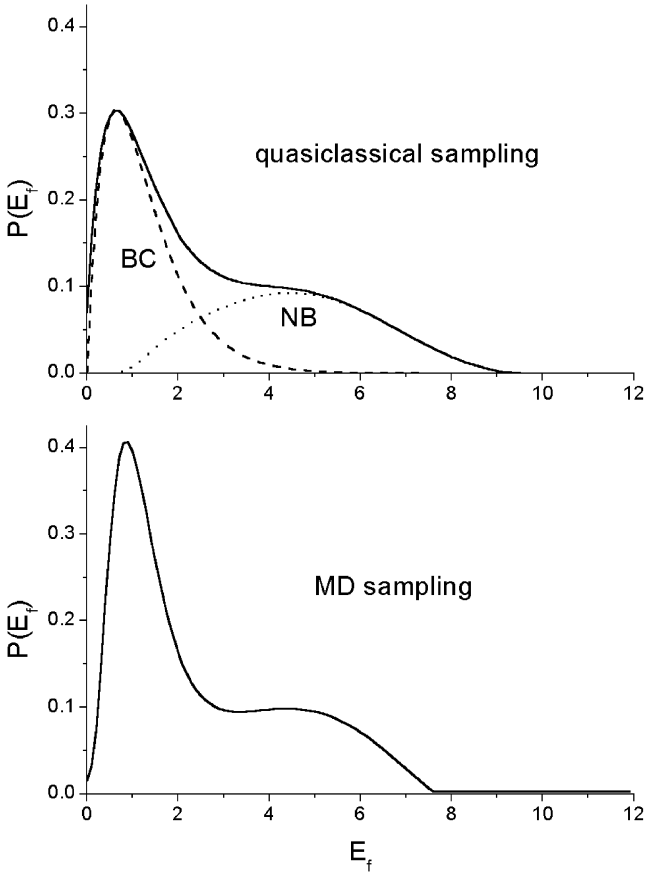

Figure 8. Comparison of quasiclassical and MD sampling for the surface at 0 K, using the UA-small/Au-1-stiff surface model and the Ne-IV(UA) potential.

sampling. Average results of the trajectories are listed in Table 6. The $P(E_f)$ distribution for quasiclassical sampling is given in Figure 6. The other distributions are shown in Figures 7 and 8.

The energy-transfer dynamics is not strongly dependent on the sampling method used to choose initial conditions for the surface. For T of both 293 and 0 K, $\langle E_f \rangle$ is somewhat larger for quasiclassical sampling than that for MD sampling, but the difference is rather small. Similarly, the Boltzmann component is larger for MD sampling. These differences are consistent with a lower initial energy content in the SAM surface for MD sampling as compared to quasiclassical sampling. However, given the approximately factor of 2 initial energy content of the surface for quasiclassical sampling, the energy-transfer dynamics for the two sampling methods are rather small.

The insensitivity of the energy-transfer dynamics to the surface temperature, that is, 293 or 0 K, mirrors the comparison between quasiclassical and MD sampling. There is more energy transfer to the surface for the initial surface temperature of 0 K, but the difference with the 293 K results is quite small.

C. Comparison of Models for the Au{111} Surface. Average energy-transfer results for different models of the Au{111} surface are listed in Table 7. The energy-transfer distribution, $P(E_f)$, is similar for all of the simulations and is shown in Figure 7a for the Au-1-stiff model. The properties of the Au{111} surface model considered in the simulations are one or two gold layers, the gold atom potential represented by an artificially stiff force field, the universal force field (UFF), or the many-body Sutton−Chen (SC) potential, a single-layer model of Au atoms treated the same as the SAM surface, as a thermal bath, or as a rigid layer, and a two-layer model of Au atoms with the outer layer held rigid and the inner layer treated the same as the SAM surface or as a thermal bath. The results in Table 7 show that, within the statistical uncertainties, the different models for the Au{111} surface give the same results. Thus, for this Ne + *n*-hexylthiolate SAM/Au{111} system, the same energy-transfer dynamics is found for a single, rigid-layer model for Au{111} as for a two-layer model with the outer layer held rigid and the inner layer treated as a thermal bath. The results are insensitive to the details of the model for the Au{111} surface.

TABLE 7: Effect of Different Models for the Au{111} Surface[a]

model	$\langle E_f \rangle$[b]	%BC[b]	T_{BC}[b]	%MITPs[b]	$\langle E_f \rangle_{MITPs}$[b]
Au-1-stiff	2.65 ± 0.13[c]	67.5	420	9.4	1.54 ± 0.28[c]
Au-1-stiff(bath)	2.73 ± 0.12	66.5	450	8.5	1.50 ± 0.26
Au-1-rigid	2.71 ± 0.12	63.5	430	11.7	1.47 ± 0.18
Au-2-UFF	2.76 ± 0.11	68.0	460	9.8	1.32 ± 0.16
Au-2-UFF(bath)	2.82 ± 0.13	62.0	430	9.1	1.44 ± 0.25
Au-2-SC	2.63 ± 0.13	68.0	430	8.3	1.20 ± 0.21
Au-2-SC(bath)	2.53 ± 0.13	73.0	430	8.9	1.13 ± 0.19

[a] The simulations were performed with the UA-small SAM model and the Ne-IV(UA) Ne + SAM potential. MD sampling was used to choose initial conditions for the SAM. [b] BC is the Boltzmann component and %BC is the percent of $P(E_f)$ that is represented by eq 1. T_{BC} is the temperature (K) for Boltzmann component, eq 1, of $P(E_f)$. %MITPs is the percent of the trajectories with multiple inner turning points (MITPs). $\langle E_f \rangle_{MITPs}$ is the $\langle E_f \rangle$ for trajectories with MITPs. [c] Uncertainty is for a 95% confidence interval.

IV. Summary

There is much interest in understanding the dynamics associated with collisions of rare-gas atoms with hydrocarbon films, including self-assembled monolayers (SAMs). In the work presented here, a range of attributes of the molecular dynamics model for Ne atoms colliding with a *n*-hexylthiolate SAM/Au{111} surface are adjusted to determine how they affect the energy-transfer dynamics. The following are the principle findings of this study.

(1) The interaction of a Ne atom with the hydrogen and carbon atoms of the SAM is represented by the Ne + CH_4 intermolecular potential determined from ab initio theory. The Ne + *n*-hexylthiolate SAM energy-transfer dynamics are insensitive to the details of the analytic function used to represent the ab initio potential. A fitting function that includes both two-body and three-body terms gives the same results as one that only includes the former terms.

(2) The Ne + CH_4 potential calculated at the MP4/aug-cc-pVTZ level of theory is in excellent agreement with experiment.

(3) United-atom (UA) models for the CH_3 and CH_2 moieties of the SAM were determined from isotropic averages of explicit-atom (EA) models of the Ne + CH_4 potential. The EA model gives approximately 10% less energy transfer to the SAM in Ne + SAM collisions than does its UA representation. Previous trajectory simulations[12−14] of Ne + SAM/Au{111} collisions used a UA model determined from the QCISD(T)/6-311++G-(d,p) potential curve for Ne interacting with the face of CH_4. This UA model gives energy transfer results nearly the same as those given by the UA model derived here from the isotropic average of the MP4/aug-cc-pVTZ potential for Ne + CH_4. There are several reasons for the less-efficient energy accommodation with the EA SAM model. With the H atom explicitly represented, there are increased repulsive interactions arising from the H atoms. Thus, the EA SAM is denser and stiffer than the UA model. With its relatively less-stiff structure, the UA SAM model has lower barriers for conformational changes, for

example, from trans to gauche dihedral angle for an alkyl chain. Therefore, the UA SAM absorbs the collision energy more easily by conformational changes than does the EA model.

(4) A SAM consisting of only 35 $CH_3(CH_2)_5S$ chains gives the same result as does a much larger model with 100 chains. The Ne + SAM/Au{111} energy-transfer dynamics may be represented by a rather small model for the SAM.

(5) Quasiclassical and molecular dynamics samplings of initial conditions for the SAM give very similar energy-transfer dynamics, even though the former includes zero-point energy and the latter is purely classical without zero-point energy added. The initial total energy of the SAM/Au{111} surface is approximately a factor of 2 larger with quasiclassical sampling. However, this has no significant effect on the Ne + SAM/Au{111} energy transfer.

(6) Energy transfer in Ne + SAM/Au{111} collisions is insensitive to whether one or two layers of gold atoms are used to represent the Au{111} surface, whether the single layer is treated as rigid or as a thermal bath, or whether the potential of the gold atoms is represented by the two-body universal force field (UFF) or the Sutton−Chen many-body potential.

The comparisons made here show that the UA-small/Au-1-stiff/Ne-V(UA) model used previously[12−14] to simulate collisions of Ne atoms with the *n*-hexylthiolate SAM/Au{111} surface is adequate for studying the dynamics of the collisional energy transfer and comparing with experiment. However, even more quantitative comparisons with experiment may be possible by using an explicit-atom (EA) model for the SAM and a more accurate Ne−SAM potential. The simulations reproduce the experimental energy distribution, $P(E_f)$, of the scattered Ne atoms.[15,16] By studying details of the trajectories, it should be possible to determine the origin of Boltzmann and non-Boltzmann components of $P(E_f)$.

Acknowledgment. The research presented here was funded by the National Science Foundation.

References and Notes

(1) Ulman, A. *An Introduction to Organic Films*; Academic Press: San Diego, CA, 1991.

(2) Ulman, A. *Chem. Rev.* **1996**, *96*, 1533.

(3) Poirier, G. E. *Chem. Rev.* **1997**, *97*, 117.

(4) Fenter, P.; Schreiber, F.; Berman, L.; Scoles, G.; Eisenberger, P.; Bedzyk, M. J. *Surf. Sci.* **1998**, *412/413*, 213.

(5) Shevade, A. V.; Zhou, J.; Zin, M. T.; Jiang, S. *Langmuir* **2001**, *17*, 7566.

(6) Sadreev, A. F.; Sukhinin, Y. V. *Phys. Rev. B* **1996**, *54*, 17966.

(7) Toerker, M.; Staub, R.; Fritz, T.; Schmitz-Hubsch, T.; Sellam, F.; Leo, K. *Surf. Sci.* **2000**, *445*, 100.

(8) Mikulski, P. T.; Harrison, J. A. *Tribol. Lett.* **2001**, *10*, 29.

(9) Clear, S. C.; Nealey, P. F. *J. Chem. Phys.* **2001**, *114*, 2802.

(10) Salmeron, M. *Tribol. Lett.* **2001**, *10*, 69.

(11) Cohen, S. R.; Naaman, R.; Sagiv, J. *Phys. Rev. Lett.* **1987**, *58*, 1208.

(12) Bosio, S. B. M.; Hase, W. L. *J. Chem. Phys.* **1997**, *107*, 9677.

(13) Yan, T.-Y.; Hase, W. L. *Phys. Chem. Chem. Phys.* **2000**, *2*, 901.

(14) Yan, T.-Y.; Hase, W. L. *Chem. Phys. Lett.* **2000**, *329*, 84.

(15) Minton, T. K. Private communication, 2001.

(16) Isa, N. S.; Sibener, S. Atomic oxygen erosion of decanethiol SAMs: A molecular beam and STM study. Presented at the 222nd National Meeting of the American Chemical Society, Chicago, IL, August 26−30, 2001.

(17) Baer, T.; Hase, W. L. *Unimolecular Reaction Dynamics. Theory and Experiments*; Oxford: New York, 1996.

(18) Kennard, E. H. *The Kinetic Theory of Gases*; McGraw-Hill: New York, 1938.

(19) Hwang, G. S.; Anderson, C. M.; Gordon, M. J.; Moore, T. A.; Minton, T. K.; Giapis, K. P. *Phys. Rev. Lett.* **1996**, *77*, 3049.

(20) Minton, T. K.; Giapis, K. P.; Moore, T. *J. Phys. Chem. A* **1997**, *101*, 6549.

(21) Grimmelmann, E. K.; Tully, J. C.; Cardillo, M. J. *J. Chem. Phys.* **1980**, *72*, 1039.

(22) Lipkin, N.; Gerber, R. B.; Moiseyev, N.; Nathanson, G. M. *J. Chem. Phys.* **1994**, *100*, 8408.

(23) Benjamin, I.; Wilson, M.; Pohorille, A. *J. Chem. Phys.* **1994**, *100*, 6500.

(24) Någård, M. B.; Markovic, N.; Pettersson, J. B. C. *J. Chem. Phys.* **1998**, *109*, 10350.

(25) Arumainayagam, C. R.; Madix, R. J.; McMaster, M. C.; Suzawa, V. M.; Tully, J. C. *Surf. Sci.* **1990**, *226*, 180.

(26) Head-Gordon, M.; Tully, J. C.; Rettner, C. T.; Mullins, C. B.; Auerbach, D. J. *J. Chem. Phys.* **1991**, *94*, 1516.

(27) Stinnett, J. A.; Weaver, J. F.; Madix, R. J. *Surf. Sci.* **1997**, *380*, 489.

(28) Bolton, K.; Svanberg, M.; Pettersson, J. B. C. *J. Chem. Phys.* **1999**, *110*, 5380.

(29) Yan, T.-Y.; Hase, W. L. *J. Phys. Chem. A* **2001**, *105*, 2617.

(30) Garton, D. J.; Minton, T. K.; Alagia, M.; Balucani, N.; Casavecchia, P.; Volpi, G. G. *J. Chem. Phys.* **2000**, *112*, 5975.

(31) Minton, T. K.; Garton, D. J. Dynamics of Atomic-Oxygen-Induced Polymer Degradation in Low Earth Orbit. In *Chemical Dynamics in Extreme Environments: Advanced Series in Physical Chemistry*; Dressler, R. A., Ed.; World Scientific: Singapore, 2001; p 420.

(32) Steinfeld, J. I.; Francisco, J. S.; Hase, W. L. *Chemical Kinetics and Dynamics*, 2nd ed.; Prentice Hall: Upper Saddle River, NJ, 1999.

(33) Chapman, S.; Bunker, D. L. *J. Chem. Phys.* **1975**, *62*, 2890.

(34) Hase, W. L.; Ludlow, D. M.; Wolf, R. J.; Schlick, T. *J. Phys. Chem.* **1981**, *85*, 958.

(35) Allen, M. P.; Tildesley, D. J. *Computer Simulation of Liquids*; Oxford: New York, 1987.

(36) Hautman, J.; Klein, M. L. *J. Chem. Phys.* **1989**, *91*, 4994.

(37) Mar, W.; Klein, M. L. *Langmuir* **1994**, *10*, 188.

(38) Meroueh, O.; Hase, W. L. *Phys. Chem. Chem. Phys.* **2001**, *3*, 2306.

(39) Porter, M. D.; Bright, T. B.; Allara, D. L.; Chidsey, C. E. D. *J. Am. Chem. Soc.* **1987**, *109*, 3559.

(40) Camillone, N., III; Chidsey, C. E. D.; Eisenberger, P.; Fenter, P.; Li, J.; Liang, K. S.; Liu, G.-Y.; Scoles, G. *J. Chem. Phys.* **1993**, *99*, 744.

(41) Berendsen, H. J. C.; Postma, J. P. M.; Gunsteren, W. F. v.; Dinola, A.; Haak, J. R. *J. Chem. Phys.* **1984**, *81*, 3648.

(42) Rappe, A. K.; Casewit, C. J.; Colwell, K. S.; Goddard, W. A.; Skiff, W. M. *J. Am. Chem. Soc.* **1992**, *114*, 10024.

(43) Sutton, A. P.; Chen, J. *Philos. Mag. Lett.* **1990**, *61*, 139.

(44) Rafii-Tabar, H.; Sutton, A. P. *Philos. Mag. Lett.* **1991**, *63*, 217.

(45) Lynden-Bell, R. M. *Surf. Sci.* **1991**, *259*, 129.

(46) Frisch, M. J.; Trucks, G. W.; Schlegel, H. B.; Scuseria, G. E.; Robb, M. A.; Cheeseman, J. R.; Zakrzewski, V. G.; Montgomery, J. A., Jr.; Stratmann, R. E.; Burant, J. C.; Dapprich, S.; Millam, J. M.; Daniels, A. D.; Kudin, K. N.; Strain, M. C.; Farkas, O.; Tomasi, J.; Barone, V.; Mennucci, B.; Cossi, M.; Adamo, C.; Jaramillo, J.; Cammi, R.; Pomelli, C.; Ochterski, J.; Petersson, G. A.; Ayala, P. Y.; Morokuma, K.; Malick, D. K.; Rabuck, A. D.; Raghavachari, K.; Foresman, J. B.; Ortiz, J. V.; Cui, Q.; Baboul, A. G.; Clifford, S.; Cioslowski, J.; Stefanov, B. B.; Liu, G.; Liashenko, A.; Piskorz, P.; Komaromi, I.; Gomperts, R.; Martin, R. L.; Fox, D. J.; Keith, T.; Al-Laham, M. A.; Peng, C. Y.; Nanayakkara, A.; Challacombe, M.; Gill, P. M. W.; Johnson, B.; Chen, W.; Wong, M. W.; Andres, J. L.: Gonzalez, C.; Head-Gordon, M.; Replogle, E. S.; Pople, J. A. *Gaussian 99*, revision B.08+; Gaussian, Inc.: Pittsburgh, PA, 2000.

(47) Boys, S. F.; Bernardi, F. *Mol. Phys.* **1970**, *19*, 553.

(48) Woon, D. E. *J. Chem. Phys.* **1994**, *100*, 2838.

(49) Yin, D.; MacKerell, A. D., Jr. *J. Phys. Chem.* **1996**, *100*, 2588.

(50) Gao, D.-Q.; Chen, L.-J.; Li, Z.-R.; Tao, F.-M.; Pan, Y.-K. *Chem. Phys. Lett.* **1997**, *277*, 483.

(51) Buck, U.; Kohlhase, A.; Secrest, D.; Phillips, T.; Scoles, G.; Grein, F. *Mol. Phys.* **1985**, *55*, 1233.

(52) Axilrod, B. M.; Teller, E. *J. Chem. Phys.* **1943**, *11*, 299.

(53) Liuti, G.; Pirani, F.; Buck, U.; Schmidt, B. *Chem. Phys.* **1988**, *126*, 1.

(54) Wangler, M.; Roth, D. A.; Winnewisser, G.; Pak, I.; McKellar, A. R. W. *Can. J. Phys.* **2001**, *79*, 423.

(55) Hase, W. L.; Duchovic, R. J.; Hu, X.; Kormonicki, A.; Lim, K.; Lu, D.-H.; Peslherbe, G. H.; Swamy, K. N.; Linds, S. R. V.; Varandos, A. J. C.; Wang, H.; Wolf, R. J. *QCPE* **1996**, *16*, 671.

(56) Hase, W. L.; Darling, C. L.; Zhu, L. *J. Chem. Phys.* **1992**, *96*, 8295.